Polymer Nanocomposite Coatings for CO_2 Pipeline Corrosion Control: A Comprehensive Review

Jerome Oloto, Simbarashe Kapfudzaruwa and S.D. Jacob Muthu*

Faculty of Engineering and Applied Science, 3737 Wascana Parkway, University of Regina, Regina, SK, Canada

Abstract: Carbon dioxide (CO_2) is the most significant greenhouse gas, accounting for 77% of global warming and is produced by the combustion of fossil fuels in industries. Carbon capture, storage and utilization (CCUS) is a possible pathway in achieving the emission reduction target set by the Canadian government in 2050. The transportation of the captured CO_2 to storage is a critical factor in the CCUS process, which is frequently hindered by corrosion. The impurities in CO_2 lead to corrosion risks, which are generally addressed using inhibitors, corrosion-resistant alloys, and polymer coatings in the oil and gas sector. However, CO_2 corrosion is more complex than CO_2 sweet corrosion. It is difficult to obtain a single inhibitor capable of mitigating CO_2 corrosion in pipelines, and corrosion-resistant alloys are too expensive to be used throughout all sections of the pipeline. Polymers are employed as coatings. For gaseous and supercritical CO_2, which leads to defects in the coatings, such as blisters and porosity. As a result, researchers have focused on using nanocomposite coatings to control CO_2 corrosion. This review paper focused on the interactions of CO_2 with impurities on polymer and polymer nanocomposites. In particular, the most commonly used clay and graphene polymer nanocomposites coatings and their interactions with CO_2 were discussed. Further, the transport properties of CO_2 through polymers and polymer nanocomposites and the interaction mechanism were analyzed. The paper concludes with the processing methods used for the polymer and polymer nanocomposite coatings.

Keywords: Polymer, Polymer nanocomposite, Coating methods, Corrosion Control, CO_2 with impurities.

1. BACKGROUND

1.1. Carbon Capture, Utilization, and Storage

Climate change poses a significant global concern, contributing to environmental disasters, such as heatwaves, storms, and floods, which result in loss of life and economic challenges globally [1]. The Paris Agreement identified greenhouse gases (GHGs) as the main drivers of climate change, with countries committing to a 45% reduction in emissions by 2030. Canada, in support of these global efforts, enacted the Net-Zero Emissions Accountability Act, targeting net-zero emissions by 2050. According to the Intergovernmental Panel on Climate Change (IPCC), atmospheric carbon dioxide (CO_2) levels could reach up to 570 parts per million (ppm) by 2100, potentially increasing the average global temperature by 1.9 °C and causing sea levels to rise by up to 38 meters [2-6]. To mitigate the catastrophic effects of global warming, the IPCC emphasizes a 50- 80% reduction in global GHG emissions by 2050 [7-10].

Carbon dioxide (CO_2), the most significant GHG, is a key target for mitigation strategies such as carbon capture, utilization, and storage (CCUS). The CCUS systems are generally categorized into two stages:

1. Capture and separation of CO_2
2. Transportation and storage of CO_2

CO_2 capture technologies are classified into three main types: [2]

1. Post-combustion capture
2. Pre-combustion capture
3. Oxy-fuel combustion capture

The captured CO_2 must be transported to storage sites or utilized in various engineering applications, making the design of reliable transportation and storage systems essential. However, industrial CO_2 streams often contain impurities due to fuel types, oxidant excess, and the specific purification process used [1].

Post-combustion capture extracts CO_2 after fuel combustion. Nitrogen (N_2) is typically the most abundant impurity, resulting from excess combustion air or nitrogen oxides (NO_x) conversion. Other impurities, including oxygen (O_2) and argon (Ar), water vapour (from solvent and combustion), carbon monoxide (CO), sulphur oxides (SO_x), if coal is used. Pre-combustion capture generates CO_2 by reacting fossil fuel with air to form syngas, which contains CO, hydrogen (H_2), and water (H_2O). CO reacts with steam

*Address correspondence to this author at the Faculty of Engineering and Applied Science, 3737 Wascana Parkway, University of Regina, Regina, SK, Canada; E-mail: Jacob.muthu@uregina.ca

E-ISSN: 1929-5995/25

Table 1: Impurities Expected from Various CO_2 Capture Methods [3]

Impurities	Post-combustion (%)	Pre-Combustion (%)	Oxy-fuel combustion (%)
CO_2	> 99	> 95.6	> 90
Oxygen (O_2)	< 0.1	trace	< 3
Water (H_2O)	0.14	0.14	0.14
Hydrogen (H_2)	trace	< 3	trace
Hydrogen sulphide (H_2S)	trace	< 3.4	trace
Methane (CH_4)	< 0.01	< 0.035	-
Nitrogen (N_2)	< 0.8	balance	<1.4

to produce CO_2 and H_2. Impurities such as hydrogen sulphides (H_2S), CO, H_2O and N_2 can persist due to fuel composition, partial oxidation and solvent carryover. Oxy-fuel combustion capture uses pure oxygen instead of air, producing a flue gas mostly composed of CO_2 and water with impurities including O_2, N_2, and Ar due to excess oxygen or air ingress. Table **1** outlines the typical impurity compositions associated with each capture method.

1.2. Purification of CO_2

The captured CO_2 is further purified before being transported. In post-combustion capture, CO_2 is purified using the absorption process, either with physical solvents (e.g. selexol, rectisol) or with chemical solvents (e.g. alkanolamines, amino acids, and chilled ammonia) [4-5]. In pre-combustion, the purification of CO_2 is achieved through chemisorption (using metal oxides and salts) or cryogenic distillation. Physisorption (e.g. with zeolites or activated carbon) involves minimal changes to the adsorbent's electronic structure [6-8]. In oxy-fuel systems, purification typically employs membrane separation or cryogenic distillation. Membrane separation relies on size and affinity differences between CO_2 and other molecules. Cryogenic distillation uses low temperatures to condense, separate, and purify CO_2 from flue gases. Achieving high-purity CO_2 adds cost and energy demand to the CCUS process. While co-transporting CO_2 with impurities may reduce cost, safety regulations limit allowable impurity concentrations due to potential hazards from pipeline leaks [9]. Table **2** shows the impurity limits defined by various transport operators [10].

1.3. CO_2 Transportation

Captured CO_2 can be transported in four phases: gaseous, liquid, dense-phase, and supercritical. Supercritical CO_2 transport is generally favoured due to its cost efficiency and stability, avoiding two-phase

Table 2: Captured CO_2 Gas Stream Composition after Purification [10]

Component	Canyon Reef Pipeline	Weyburn Pipeline	Gullfaks Pipeline
CO_2	> 95%	96%	99.50%
Carbon monoxide (CO)	-	0.1%	< 10 ppm
Water (H_2O)	No free water	< 20 ppm	Water vapor
Hydrogen sulphide (H_2S)	< 1500 ppm	0.9%	-
Sulphur Oxide (SO_2)	-	-	< 10 ppm
Total Sulfur	< 1450 ppm	-	-
Nitrogen (N_2)	4%	< 300ppm	< 0.48%
Nitrogen Oxide (NO_x)	-	-	< 50 ppm
Oxygen (O_2)	<10 ppm	< 50ppm	< 10 ppm
Glycol	4×10^{-5} Lm^{-3}	-	-
Methane (CH_4)	-	0.7%	-
Hydrocarbon	< 5 %	-	< 10 0ppm

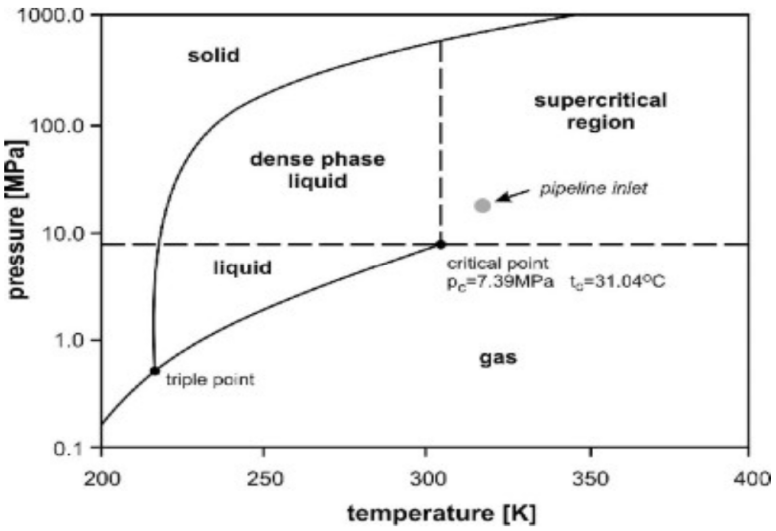

Figure 1: The Phase diagram of CO_2 [12].

flows [11-12]. Impurities in CO_2 can shift the phase boundaries, requiring higher pressure to maintain the supercritical or dense phase, as can be seen in the phase diagram (Figure **1**). The triple point (0.52 MPa, 217.15 °K), where the solid, liquid, and gas phases coexist. Above the critical point (7.38 MPa, 304.25 °K), CO_2 enters supercritical regions. Supercritical CO_2 behaves like both a liquid (high density) and a gas (low viscosity) [13-14]. CO_2 is typically compressed into a supercritical phase with a temperature above 31.10 °C and a pressure greater than 7.38 MPa [15]. The CO_2 transporting method includes pipelines (most economical for distances up to 1000-15000 km), ships, rail, and road tankers. By 2050, an estimated 2,000 km of CO_2 pipelines will be needed to transport 10 billion tons of CO_2 [16]. Though the pipeline requires a significant one-time investment, and is considered economical compared to other forms of transportation.

Pipelines are commonly constructed from carbon steel due to its mechanical strength and low cost. However, impurities, especially in the presence of water, can lead to the formation of carbonic acid (H_2CO_3), which is highly corrosive. This can result in localized corrosion, hydrogen-induced cracking, and stress corrosion cracking. Further, the threshold of impurity tolerance without compromising transportation system integrity is not fully understood. Therefore, it's critical to find a suitable preventive mechanism which could control the reaction between the impurities and the carbon steel pipeline materials.

To mitigate corrosion, polymer coatings can be applied as a protective barrier. However, polymers, especially under exposure to gaseous or supercritical CO_2, may experience issues such as swelling and plasticization, reduction in glass transition temperature and crystallization [17]. These effects can lead to blistering, porosity and delamination of coatings. Therefore, a comprehensive review is necessary to identify CO_2-resistant polymers. With advancements in nanotechnology, polymer nanocomposites, i.e. polymers reinforced with nanomaterials, offer enhanced mechanical properties and corrosion resistance. These composites are now being explored for protective coatings in CO_2 pipeline systems. Further, polymer nanocomposite (PNC) coatings are in a developing stage; as such, a critical review of PNC coatings for CO_2 corrosion control is important.

Therefore, the paper aims to review polymer and polymer nanocomposite coatings for CO_2 transportation systems. The paper begins by analyzing the interactions of polymers with gaseous and supercritical CO_2, followed by an overview of transport properties. The review then summarizes current polymer coating materials, explores nanofillers that enhance polymer performance, and discusses the transport properties. The paper concludes by analyzing the manufacturing techniques and characterization of transport properties of polymer nanocomposite coatings used for CO_2 pipelines.

2. POLYMERS USED FOR COATINGS

Polymers are macromolecules composed of long chains of repeating monomer units primarily linked through covalent bonds [18]. Based on their structure and thermal behavior, polymers are generally classified into three types: thermosets, thermoplastics and

elastomers. Thermoset polymers such as epoxy, polyurethane (PU), phenolic, and unsaturated polyester form highly cross-linked, three-dimensional network structures during curing. The high degree of cross-linking significantly restricts molecular chains' mobility, resulting in materials that are rigid, dimensionally stable, and resistant to deformation under heat and stress. Thermoplastic polymers, on the other hand, consist of linear or branched polymer chains that are physically entangled rather than chemically cross-linked. In their molten state, these chains can flow and be reshaped, allowing thermoplastics to be processed using conventional techniques such as extrusion, injection molding, and compression molding.

Thermoplastics are further classified into semi-crystalline and amorphous types based on their degree of structural order. Semicrystalline thermoplastics, including polyethylene (PE), high-density polyethylene (HDPE) and low-density polyethylene (LDPE), polypropylene (PP), polyethylene terephthalate (PET), polyamide (nylon), and polytetrafluoroethylene (PTFE or Teflon), contain both ordered crystalline domains and disordered amorphous domains. These materials exhibit a defined melting temperature (T_m) above which the crystalline regions transition to the molten state. Amorphous thermoplastics cannot crystallize due to irregular chain structures and instead are characterized by a glass transition temperature (T_g), the temperature over which they transition from a hard, glassy state to a soft, rubbery state. Representative examples include polystyrene (PS), polyvinyl chloride (PVC), acrylonitrile butadiene styrene (ABS), polycarbonate (PC), and polymethyl methacrylate (PMMA).

Elastomers are lightly cross-linked polymers that exhibit rubber-like elasticity. They can undergo large deformations under stress and return to their original shape upon unloading. Their flexible molecular structure and cross-linked network allow for excellent elastic recovery. Common elastomers include natural rubber (polyisoprene) and a wide range of synthetic rubbers such as ethylene propylene diene monomer (EPDM), styrene-butadiene rubber (SBR), polybutadiene rubber (BR), polyisoprene rubber (IR), chloroprene rubber (Neoprene), polyurethane elastomers (PU) and silicone rubber.

2.1. Interactions of CO_2 with Polymer Coatings and their Effects

2.1.1. Absorption and Swelling

Amorphous thermoplastics and elastomers have a notable capacity to absorb CO_2, which leads to polymer swelling. This phenomenon reduces polymer stiffness (resistance to elastic deformation) while enhancing toughness (resistance to crack propagation). The extent of absorption and swelling is governed by the solubility of CO_2 in the polymer matrix. Furthermore, CO_2 absorption can induce crystallization in some polymers, increasing their melting enthalpy and melting temperature [19]. The complex relationship between CO_2 absorption and polymer crystallinity is a critical factor contributing to polymer degradation under high-pressure CO_2 exposure [20]. Figure **2** shows the CO_2 sorption at 6.5 MPa in various polymeric materials.

2.1.2. Plasticization and Crystallization Phenomena

Plasticization refers to the process by which low-molecular-weight compounds, such as CO_2, diffuse into polymers, increasing chain mobility by disturbing intermolecular forces. In structurally regular polymers, this increased chain mobility can promote or enhance

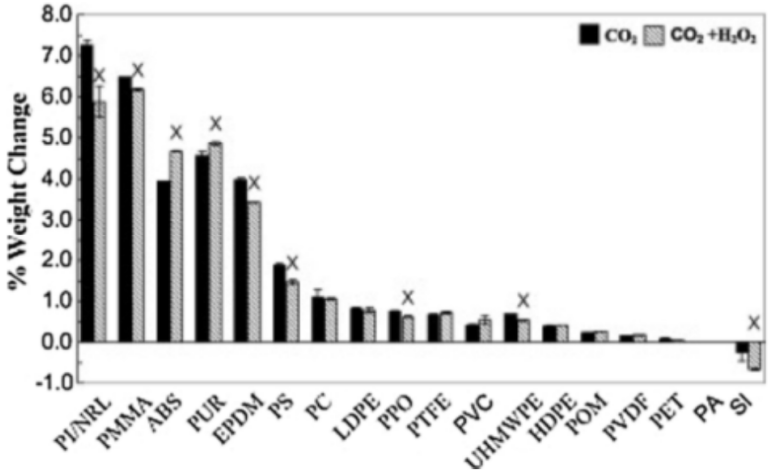

Figure 2: CO_2 sorption at 6.5 MPa in various polymeric materials [21].

crystallization, particularly during depressurization or outgassing phases [22-23]. Amorphous polymers possess greater free volume compared to semi-crystalline polymers, making them more susceptible to plasticization [24-26].

The plasticization is typically characterized by a shift in glass transition temperature, and an increase in melting temperature (T_m), melting enthalpy (ΔH) and CO_2 permeability [27]. Shieh *et al*. [28] demonstrated that the prolonged exposure of polyethylene terephthalate (PET) to supercritical CO_2 resulted in increased crystallinity as the plasticized regions transformed into an ordered crystalline domain. Sawan *et al*. [23] investigated amorphous polymers such as polymethyl methacrylate (PMMA), polyethylene terephthalate glycol-modified (PETG), and polyethylene terephthalate (PET), under supercritical CO_2 exposure. Their results showed a reduction in glass transition temperatures and an increase in T_m and ΔH, confirming enhanced crystallinity due to the plasticizing effect of CO_2 absorption.

2.1.3. Rapid Gas Decompression (RGD Damage)

Rapid gas decompression (RGD) is a significant degradation mechanism in polymers exposed to high-pressure gaseous CO_2, followed by sudden depressurization [29-30]. During decompression, the dissolved gas rapidly expands within the polymer matrix, leading to bubble nucleation, blistering, tearing, or even rupture if the gas doesn't diffuse out effectively [31-35]. Elastomers are particularly vulnerable to RGD due to their high free volume and inherent porosity from manufacturing. Dubois *et al*. [33] utilized high-pressure in-situ FTIR microscopy to study supercritical CO_2 sorption and swelling of unfilled elastomers. Their results showed that CO_2 uptake increases with pressure and temperature, especially in elastomers with polar functional groups such as carbonyl or chlorinated segments, resulting in a swelling ratio that exceeded the mass uptake.

2.1.4. Change in Mechanical Properties

CO2-induced plasticization and crystallization directly influence the mechanical properties of polymers. Shieh *et al*. [28] examined polymers such as HDPE, LDPE, and polypropylene (PP) exhibited decreased modulus of elasticity and yield strength due to plasticization. Jimenez *et al*. [21] investigated the compatibility of medical-grade polymers with dense and liquid CO_2 in the presence of aqueous hydrogen peroxide (H_2O_2), observing CO_2 uptake in amorphous polymers, while semi-crystalline polymers exhibited minimal change in tensile strength or weight. Kim *et al*. [36] further examined how gas adsorption affects mechanical behavior. Their results indicated that CO_2 acts as a plasticizing agent, enhancing impact strength at an adsorption level of 2.85%, with the peak energy absorption of 68.8 J/m after 12 hours. However, a consistent decline in tensile strength was observed with increased CO_2 uptake and longer exposure times.

2.2. Polymer Coatings for CO_2 Corrosion Control and Associated Challenges

While polymer coatings have been widely employed for corrosion control in CO_2-rich environments, they present several limitations. The main issues include blister formation, crystallization and porous structure, all of which can degrade mechanical integrity. Exposure to gaseous CO_2 or supercritical CO_2 ($SCCO_2$) can alter coating morphology, and thus, the resilient coatings tend to develop blisters, whereas brittle coatings form pores that lead to cracking and delamination.

Effective polymer coatings should possess strong adhesion to the metal substrates, high glass transition temperatures, and resistance to $SCCO_2$ or gaseous CO_2. Bierwagen [37] investigated the performance of several commercial coatings, including TZ™ 904, Scotchkote™ 345, DevChem™ 253, and Polyoil™ 130-based systems under $SCCO_2$ exposure. The findings revealed that resistance to $SCCO_2$ is closely linked to the thermal stability of the polymer. Zarkaria *et al*. [38] evaluated the performance of three epoxy-based commercial coatings under high-pressure CO2 following the NACE TM0185 standard. While all coatings withstood physical deterioration, Rust-Oleum Epoxyshield 7.1-L coating experienced a reduction in pull-off adhesion at elevated temperatures, indicating thermal degradation. Sauri *et al*. [39] assessed the suitability of phenolic epoxy (PE), fusion bonded epoxy (FBE), and fluoropolymer (FP) coatings under simulated static operational conditions for both CO_2 producer and injection wells. According to NACE T0297 standard, PE demonstrated superior performance, maintaining adhesion and hardness across both conditions. Zhang *et al*. [40] examined the corrosion behavior of S355 structural steel and 316L stainless steel in gaseous CO_2 containing 3.5% sodium chloride (NaCl) using three types of polymer coatings: phenol epoxy and two-pack vinyl ester-based systems reinforced with glass flecks. Electrochemical impedance spectroscopy (EIS) and ASTM D 4541-02 pull-off adhesion tests were conducted pre- and post-

Table 3: Comprehensive Summary of Polymer Coating for CO_2 Pipeline

Coatings/thickness (μm)	Coating method	Exposure condition	Coating Defects	Impurities	Ref
TZ™ 904 + Toluene adjusted/63- 335/	Spray Method	32 – 40 °C 1100 -1580 psi for 24 - 48 hours	Blisters, porous structure, Low adhesion, Thickness increase and low impedance.	No Impurities	[37]
DevChem™253 + xylenes adjusted/52 -165					
Scotchkote™323 (S323) S323 base and S323 hardener + xylenes adjusted/ 35 -172					
Scotchkote™ 345 (S345) + Xylene adjusted/15 - 180	Spray Method	32 – 40 °C 1100 -1580 psi for 24 - 48 hours	No change in the coating, thickness and weight remained constant, Impedance remained the same except for the thin film.		
Polyoil™-130-based coatings/12-151	Spray Method	32 – 40 °C 1100 -1580 psi for 24 - 48 hours	Blisters appeared at the surface and disappeared when the temperature of the cure increased. The porous structure of the two coating formulations, thickness and weight remained constant. Impedance decreased when the exposure time increased.		
Finitec Solidex Water-Based Protective Floor Coating / not listed	-	25 - 80 °C 2175.57 psi For 28 days	No defect	No impurities	[38]
Rust-Oleum Epoxy Shield Glossy Grey Water-Based Garage Floor Coating	-				
Rust-Oleum Epoxyshield 7.1-L Glossy Grey Garage Floor Coating Kit	-		Reduction in adhesion strength	No impurities were present	[48]
Phenolic Epoxy Coating (PE)/400	-	135 °C, 5000 psi	No defect	H_2S 200-400 ppm with synthetic brine	[39]
Fusion Bonded Epoxy coating (FBE)/350					
Fluoropolymer coating (FP)/60					
Phenol epoxy/360	-	60 °C, 100 bar for 35 days	Delamination due to blistering at the coating/steel interface and voids. Low impedance	The flue gas was mixed in a single gas manifold – No impurities	[40]
Coating B+ 2 peck Vinyl ester reinforced with screen glass flecks/1060	-	60 °C, 100 bar for 35 days	No blisters and few voids		[40]

exposure. The corrosion rate for S355 steel was approximately 0.02 mm/year at 100 bar and 60° C, and 0.3 mm/year at 1.65 bar and 65° C when exposed to CO_2 derived from flue gas [40]. Table **3** summarises the performance of various polymer coatings for CO_2 pipeline applications. In summary, although polymer coatings have demonstrated effectiveness in mitigating corrosion in CO_2 transportation systems, several inherent drawbacks such as blistering, plasticization-induced property degradation, RGD damage, and porosity necessitated the development of new materials. To address these challenges, advanced materials, particularly polymer nanocomposites, are being explored for enhanced mechanical and chemical stability under CO_2-rich environments.

3. POLYMER NANOCOMPOSITE COATINGS

Recent advancements in nanomaterials have enabled significant improvements in the performance of

polymer coatings by incorporating impermeable nanofillers with high aspect ratios. These fillers disrupt the diffusion pathway of gas molecules, resulting in a reduced diffusion rate and increased diffusion time [41, 42]. The inclusion of such nanofillers in polymer matrices decreased the available diffusion areas and enhanced the tortuosity of diffusion pathways. Consequently, polymer nanocomposite (PNC) coatings can mitigate blistering, control plasticization and crystallization and reduce porosity under CO_2 exposure. Functionalized nanomaterials can also improve coating adhesion to substrates, thereby minimizing the risk of delamination. Properly engineered nanocomposite coatings can effectively act as barriers, preventing CO_2 and its impurities from reaching and corroding metallic surfaces.

Several factors influence the characteristics and performance of polymer nanocomposite coatings [43]:

- Filler attributes: volume fraction, shape, concentration, and aspect ratio
- Polymer characteristics: crystallinity, permeability, and intrinsic barrier properties,
- Filler dispersion: orientation, agglomeration, distribution, and interfacial interactions within the matrix

3.1. Polymer Nanocomposites and their Interaction with CO_2

Among the various nanofillers, clay minerals (e.g., kaolinite, bentonite, montmorillonite, cloisite, vermiculite, mica, halloysite, and talc) [44-47], layered silicate [48-49], graphene derivates [50], cellulose nanocrystals [44-51], silica nanoparticles [52-53] have demonstrated significant potential for enhancing polymer barrier properties. Clays and graphene are among the most widely studied due to their high aspect ratio and compatibility with various polymers [54-57]. Therefore, this section focuses on polymer nanocomposite coatings reinforced with clay and graphene nanofillers under a CO_2 environment.

3.1.1. Nanoclay-Polymer Nanocomposite Coatings

Clay-reinforced polymer nanocomposites offer excellent barrier properties by significantly reducing the permeability of gases, water, and hydrocarbons [58-59]. These improvements are strongly influenced by the dispersion of nanoclay within the polymer matrix and the strength of the polymer-filler interfacial interactions [60-61]. However, the nanoclays are hydrophilic and prone to agglomeration due to van der Waals interactions, necessitating surface modification to ensure uniform dispersion [62]. Common modification techniques included hydrophobic treatment [63], intercalation [64-66], and exfoliation [65]. Manninen *et al*. [67] evaluated CO_2 sorption and diffusion in polymethylmethacrylate (PMMA) reinforced with organoclay (cloisite 20A-(C20A)). Their result indicated that organoclay did not alter CO_2 solubility, but increased diffusion coefficients due to poor dispersion and clay agglomeration. Similarly, Guo *et al*. [68] demonstrated that C20A dispersion significantly influences CO_2 permeability in polystyrene-based nanocomposites. Hu *et al*. [69] investigated the gas transport properties of isotactic polypropylene (IPP)/nano montmorillonite (MMT) composites. Increased MMT loading led to lower swelling ratios and reduced CO_2 diffusion coefficients due to the hindrance of chain mobility and free volume by crystalline regions.

3.1.2. Graphene-Polymer Nanocomposite Coatings

Graphene, with its two-dimensional hexagonal carbon lattice, exhibits exceptional impermeability to gases, along with superior mechanical, thermal and electrical properties. When uniformly dispersed in polymers, graphene enhances gas barrier performance more effectively than clay layers [70]. Ouyang *et al*. [71] demonstrated that graphene oxide (GO) - graphene sandwich nanopaper could completely block CO_2 permeation through 12 μm thick-films. Roilo [72] investigated epoxy nanocomposites containing few-layer graphene (FLG) and found that increasing FLG content reduced free volume and gas permeability, without affecting solubility. These findings highlighted the critical role of filler content and dispersion in achieving effective CO_2 barriers.

3.2. Permeation Properties of CO_2 through Polymer Coatings

Characterization of the permeation properties will assist in selecting suitable coating materials.

3.2.1. Permeation

Gas permeation in dense, nonporous films follows a solution-diffusion mechanism, governed by Henry's law and Fick's law. Permeation is influenced by polymer type, crystallinity, thermal history and testing temperature [73-74]. Flaconneche *et al*. [75] studied the permeation of various gases (helium, argon, nitrogen, methane, and CO_2) through polyethylene

(PE), polyamide II (PA11), and polyvinylidene fluoride (PVF2), finding that CO_2 permeability was highest in PE and increased with temperature due to enhanced chain mobility.

3.2.2. Solubility

Gas solubility refers to the equilibrium concentration of gas in a polymer under specific conditions. It is quantified by the solubility coefficients (S), which vary with temperature and polymer structure. Ansaloni *et al*. [19] investigated the liquid CO_2 affinity in thermoplastic polymers (e.g., polytetrafluoroethylene (PTFE) and high-density polyethylene) and elastomers. Their results identified that elastomers experienced higher CO_2 uptake, resulting in significant volumetric swelling. Shieh *et al*. [28] found that polymer chemical structure strongly affects CO_2 solubility. Polyvinylidene fluoride (PVDF) and nylon 66 exhibited CO_2 uptake due to fluorine and amide group interactions, respectively. Flaconneche *et al*. [75] further confirmed that solubility is also influenced by polymer crystallinity and thermal history. Figure **3** shows the solubility of liquid CO_2 in different polymers.

3.2.3. Diffusivity

Gas diffusivity depends on the concentration gradients and is influenced by free volume (Figure **4**), molecular structure, penetrant size and temperature. According to Arrhenius' law, the diffusivity is defined as

$$D = D_0 \exp\left(\frac{-E_D}{RT}\right) \quad (1)$$

Flaconneche *et al*. [75] reported that higher CO_2 diffusion in plasticized PA 11 is due to increased chain mobility. They also identified that diffusion coefficients increased with temperature and gas molecule sizes.

3.3. Permeation Properties

The relationship between permeability (P), diffusivity (D), and solubility (S) can be defined as given below [74-76].

The flux, J, of the gas in a polymer matrix can be defined as

$$J = \frac{Q}{At} \quad (2)$$

Further, the flux, *J* is directly proportional to the gradient of the gas concentration, C and is defined as

$$J = -D\nabla C \quad (3)$$

The change of flux per film's thickness is equal to the rate of change of concentration and is given as

$$-\frac{dJ}{dx} = \frac{dC}{dt} \quad (4)$$

Fick's second law can be obtained by combining Equations. [3-4] with constant D in the coatings

$$-\frac{dC}{dt} = -D\frac{d^2C}{dx^2} \quad (5)$$

For a coating thickness of *l*, the flux can be obtained by integrating the flux equation (Eq. 3).

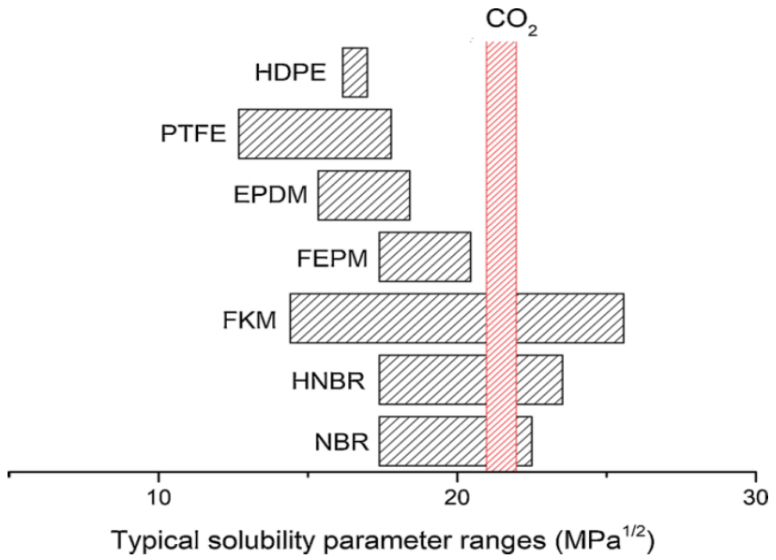

Figure 3: Solubility characteristics of polymers and liquid CO_2 at room temperature [19].

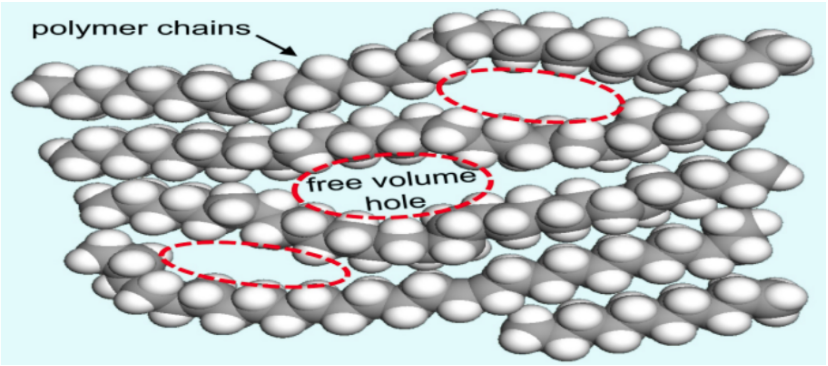

Figure 4: Free volume in polymer [72].

$$J\int_0^l dx = -D\int_{C_1}^{C_2} dC \quad (6)$$

$$J = D\frac{C_1 - C_2}{l} \quad (7)$$

C_1 and C_2 are the gas concentrations in the coatings close to the sample's face. The concentration, C, is linked to the partial pressure (p) and solubility (S) by Henry's law [77 - 84] and is given by

$$C = Sp \quad (8)$$

This results in the flux, *J*,

$$J = \frac{DS(p_1 - p_2)}{l} \quad (9)$$

$$Permeability\ P = DS \quad (10)$$

Using the time lag method and based on the pressure gradient at the permeation side under steady state conditions, the diffusion coefficient is given as.

$$D = \frac{l^2}{60} \quad (11)$$

The permeability P is defined using a time lag approach

$$P = \frac{M_w Vl}{p_{i,f}\rho RTA}\frac{dp_i}{dt} \quad (12)$$

Where

- D is the diffusivity given by cm^2/s
- S is the solubility given by the ratio of the gas concentration in the polymer to the pressure in $cm^3(STP)/cm^3$
- P is the permeability given by $cm^3(STP)/cm^3$ MPa
- p_f is the feed pressure (cmHg)
- *V* is the volume on the permeate side (cm^3)
- *A* is the area of the film (cm^2)
- *t* is the time (sec)
- *Q* is the volume flux (cm^3/s)
- R is the universal gas constant (cm^3. cmHg/gmol.K)
- T is the temperature (K)
- M_w is the molecular weight of the penetrant (g/mol)
- ρ is the density of the penetrant (g/cm^3)
- *l* is the thickness of the film (cm)
- *dpi/dt* is the pressure gradient (cmHg/s)

The solubility coefficient, S, can be calculated using the diffusion and permeability coefficients. [85-86].

3.4. Transport Properties of Polymer Nanocomposites

Similar to polymer, PNCs follow the solution-diffusion model due to the pressure gradient across the nanocomposite coatings [87]. Gas permeability can be measured using the time lag or constant-volume methods.

3.4.1. Solubility and Diffusion Coefficient

Picard *et al*. [88] presented the penetrant solubility for nanocomposite (S_c) as:

$$S_C = S(1-\phi) \quad (13)$$

The diffusion coefficient of the nanocomposite (D_c) can be obtained by

$$D_C = \frac{D}{60} \quad (14)$$

The permeability coefficient for the nanocomposite (P_c) can be written as:

$$P_C - DS(1-\phi)f \quad (15)$$

Where,

- ø is the volume fraction of the nanofiller-reinforced polymer matrix.
- *f* is the tortuosity factor

3.4.2. Tortuosity Factor

The Maxwell model predicted the tortuosity factor for a nanocomposite coating reinforced with a periodic array of impermeable spheres [89].

$$f = 1 + \frac{1 + \left(\frac{\phi}{2}\right)}{1-\phi} \quad (16)$$

The model prediction is good for a 10% volume of spherical particles. The model was further improved by adding a periodic array of infinite cylinders embedded with parallel nanofillers [90] and given by

$$f = 1 + \frac{(1+\phi)}{(1-\phi)} \quad (17)$$

For a nanocomposite film with nanoparticles oriented perpendicular to the diffusion path, the tortuosity factor was calculated using Nielsen's model [91] and given as:

$$f = 1 + \phi\frac{l_p}{2l_p} \quad (18)$$

Cussler *et al*. [92] assumed that Nielson's model was inadequate for a low filler volume fraction with overlap and introduced a model for nanoplatelets aligned perpendicular to the diffusion path as given below:

$$f = 1 + \frac{\alpha^2\phi^2}{4(1-\phi)} \quad (19)$$

- α^2 is the aspect ratio, which is given as $\frac{d}{a}$
- *d* is the distance of the nanoplatelets to the next.
- *a* is the thickness of the nanoplatelets.

Figure **5** illustrates the CO_2 diffusion directly through the polymer matrix and through a tortuous path created by nanoplatelets in a polymer matrix [93].

3.5. Fabrication Techniques for Polymer and Polymer Nanocomposite Coatings

Coatings applied to CO_2 pipeline materials are primarily categorized as metallic, inorganic, or organic [94], with this review focusing on organic coatings, including polymer and polymer nanocomposite coatings For effective application, substrate surface preparation is essential, as surface contaminants and roughness influence the coating adhesion. The primary fabrication techniques for polymer and nanocomposite coatings include the following:

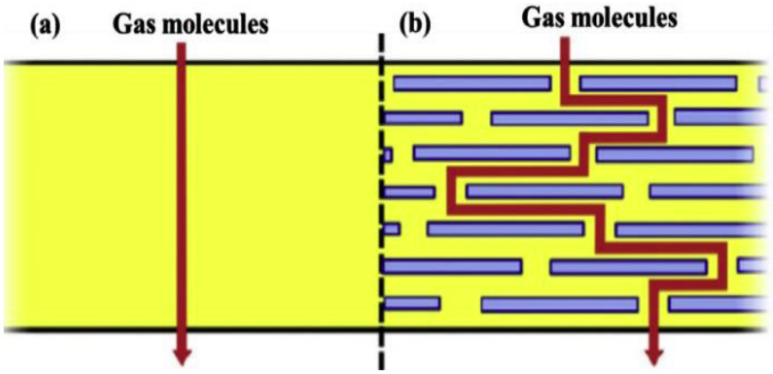

Figure 5: Schematic diagram of a gas molecule diffuses (**a**) perpendicularly through (**b**) a tortuous pathway created by nanoplatelets in a polymer matrix [93].

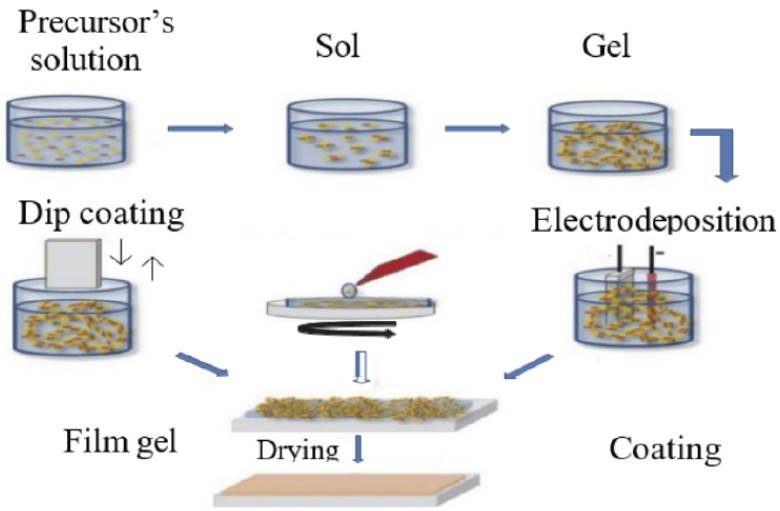

Figure 6: Sol-gel coating process [96].

3.5.1. Sol-Gel Technique

The sol-gel process, in conjunction with physical deposition methods, enables the formation of a uniform coating with micron-level thickness [95]. Typically, a sol is prepared by dissolving a precursor (e.g., calcium phosphate) in a mixture of methanol and distilled water. Heating facilitates gelation by increasing viscosity. Coatings are then applied by dip-coating, exhibiting excellent adhesion, compositional tunability, and compatibility with complex geometries. However, limitations include long processing times, sensitivity to layer thickness (risk of cracking), and potential phase separation during thermal curing. Figure **6** shows the sol-gel coating process.

Facio *et al*. [97] produced superhydrophobic surface coatings via the sol-gel process using silica nanoparticles and silanol-based precursors. The densely packed coating traps air and prevents water droplets from penetrating. Hybrid approaches, such as electrochemical codeposition combined with sol-gel, have enabled the incorporation of nanoparticles like gold [98].

3.5.2. Electrostatic Powder Coating

This solvent-free method utilizes an electrostatic spray to deposit dry powders onto a grounded substrate, followed by curing in an oven at elevated temperature to form a continuous film [99, 100]. Applicable to both thermoplastic (e.g., PE, PP, PVC), thermoset (e.g., epoxy, polyester) polymers and hybrid (e.g., combination of epoxy and polyester) polymers. Powder coatings offer environmental advantages such as the absence of volatile organic compounds, reduced waste and minimal toxicity. Limitations include defects like wrinkling or pinholes and challenges in coating complex geometries [99]. Figure **7** shows the electrostatic powder coating process.

3.5.3. Physical and Chemical Vapor Deposition

Physical vapor deposition (PVD) involves vapor-phase transport of atoms or molecules that condense

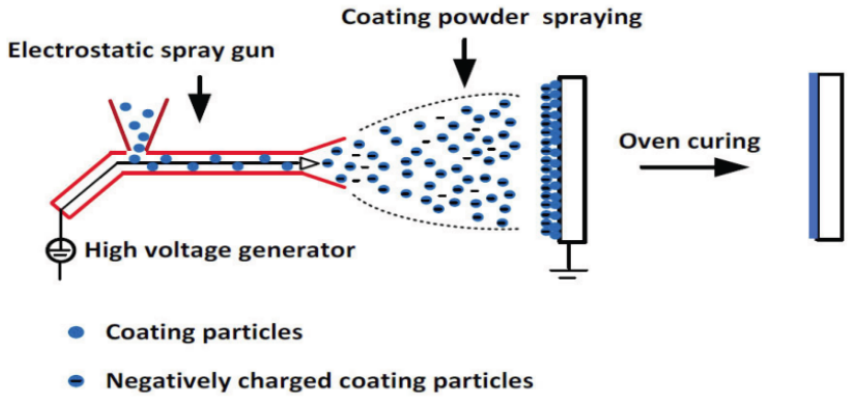

Figure 7: Electrostatic powder coating [100].

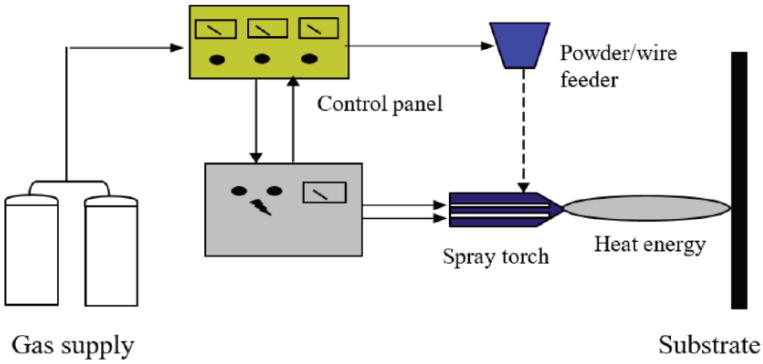

Figure 8: Thermal spray coating layout [109].

on a substrate to form coatings. PVD is suitable for depositing inorganic matrices or nanocomposite films [94]. Chemical vapor deposition (CVD) entails gas-phase chemical reactions on a heated substrate, forming solid coatings [101]. CVD supports high deposition rates and can achieve thick coatings without high vacuum systems. However, high temperatures (up to 600 °C) may limit substrate options, and the precursors involved can be hazardous. Plasma-enhanced CVD mitigated some of these drawbacks.

3.5.4. In-Situ Polymerization

This method synthesizes polymer coatings directly on substrates using monomers and initiators [101-103]. Common fillers include metal or metal oxide nanoparticles. Polymerization can be initiated via electrodeposition [104], oxidative agents [105], or photoinitiation [106-108]. This versatile technique allows for the formation of uniform nanocomposite layers.

3.5.5. Thermal Spray Coating

Thermal spray processes involve heating polymer or polymer-nanoparticle mixtures to a molten or semi-molten state and propelling them onto a substrate using high-velocity gas streams [109]. Common techniques include plasma arc, electric arc and high-velocity oxy-fuel (HVOF) spraying. The deposited splats solidify upon impact, creating thick coatings (25 µm to 2.5 mm). Advantages include wide material compatibility and recoatability. However, coating intricate geometries remains challenging [110]. Figure **8** shows the thermal spray coating process.

3.5.6. Flow Coating

Flow coating offers precise control of submicron polymer film thickness. It employs a fixed blade above a mobile stage with a defined gap [111]. Polymer or nanocomposite solutions are dragged across the substrate via capillary forces and friction between the blade and the moving platform. This method ensures uniform coating layers and is suitable for laboratory-scale applications.

4. CONCLUSION AND RECOMMENDATIONS

This review summarizes the use of polymer and polymer nanocomposite coatings for CO_2 pipeline applications, especially in carbon capture and transportation systems where CO_2 may exist with impurities (e.g., H_2O, H_2S, NO_X). While many studies focus on coatings under supercritical CO_2 or in the presence of specific impurities, broader characterization under realistic multi-component streams is still lacking. Nanofiller incorporation can enhance coatings performance, but filler selection and dispersion are critical. Elastomers, despite high crosslink density, can suffer damage under rapid gas decomposition. In contrast, PEEK and PTFE remain stable, and HDPE and PTFE demonstrate low CO_2 solubility and minimal mechanical degradation. Polymer thickness impacts diffusion time but not the solubility levels. Solubility in nanocomposites is generally governed by the base polymer, as fillers have negligible influence. Further, the size of gas molecules determines the diffusion coefficient. Gravimetric or pressure-based measurement techniques are used to measure the gas permeation characteristics. Graphene, graphene oxide, and clay with proper functionalization should be used to improve the barrier properties of polymer nanocomposites. All the empirical models used in determining the transport properties have certain limitations. Electrostatic coating has less environmental and climatic pollution during production.

RECOMMENDATIONS

1. Employ the flow stream method combined with mass spectrometry or gas chromatography to

evaluate the permeation behavior of CO_2 and impurity mixtures.

2. Use functionalized hybrid (e.g., clay-graphene combinations) with CO_2-resistant polymers (e.g., HDPE, PTFE, and PP) to enhance barrier properties.

3. Conduct electrochemical and structural analysis under supercritical CO_2 and impurity mixtures to understand synergistic effects.

4. Design coatings to mitigate corrosion mechanisms such as pitting, hydrogen embrittlement, and stress corrosion cracking.

5. Extend the duration of characterization tests and maintain constant impurity replenishment to simulate feed conditions.

6. Further investigate polymer absorption, plasticization, and crystallization phenomena to inform coating design.

These strategies will support the development of robust coatings tailored for long-term protection of CO2 pipeline infrastructure under complex operational environments.

DECLARATION OF GENERATIVE AI AND AI-ASSISTED TECHNOLOGIES IN THE WRITING PROCESS

During the preparation of this work, the author(s) utilized Grammarly for checking grammar and sentence formation. Following this tool, the author(s) reviewed and edited the content as necessary and take(s) full responsibility for the publication's content.

REFERENCES

[1] Porter RT, Fairweather M, Pourkashanian M, Woolley RM. The range and level of impurities in CO2 streams from different carbon capture sources. International Journal of Greenhouse Gas Control 2015; 36: 161-74. https://doi.org/10.1016/j.ijggc.2015.02.016

[2] Songolzadeh M, Soleimani M, Takht Ravanchi M, Songolzadeh R. Carbon dioxide separation from flue gases: a technological review emphasizing reduction in greenhouse gas emissions. The Scientific World Journal 2014; 2014(1): 828131. https://doi.org/10.1155/2014/828131

[3] Onyebuchi VE, Kolios A, Hanak DP, Biliyok C, Manovic V. A systematic review of key challenges of CO2 transport via pipelines. Renewable and Sustainable Energy Reviews 2018; 81: 2563-83. https://doi.org/10.1016/j.rser.2017.06.064

[4] Cavenati S, Grande CA, Rodrigues AE. Removal of carbon dioxide from natural gas by vacuum pressure swing adsorption. Energy & fuels 2006; 20(6): 2648-59. https://doi.org/10.1021/ef060119e

[5] David J. Economic evaluation of leading technology options for sequestration of carbon dioxide (Doctoral dissertation, Massachusetts Institute of Technology), 2000.

[6] Helwani Z, Wiheeb AD, Kim J, Othman MR. Improved carbon dioxide capture using metal reinforced hydrotalcite under wet conditions. International journal of greenhouse gas control 2012; 7: 127-36. https://doi.org/10.1016/j.ijggc.2012.01.007

[7] Lin LY, Bai H. Continuous generation of mesoporous silica particles via the use of sodium metasilicate precursor and their potential for CO2 capture. Microporous and Mesoporous Materials 2010; 136(1-3): 25-32. https://doi.org/10.1016/j.micromeso.2010.07.012

[8] D'Alessandro DM, Smit B, Long JR. Carbon dioxide capture: prospects for new materials. Angewandte Chemie International Edition 2010; 49(35): 6058-82. https://doi.org/10.1002/anie.201000431

[9] Halseid M, Dugstad A, Morland B. Corrosion and bulk phase reactions in CO2 transport pipelines with impurities: review of recent published studies. Energy Procedia 2014; 63: 2557-69. https://doi.org/10.1016/j.egypro.2014.11.278

[10] Pipitone G, Bolland O. Power generation with CO2 capture: Technology for CO2 purification. International journal of greenhouse gas control 2009; 3(5): 528-34. https://doi.org/10.1016/j.ijggc.2009.03.001

[11] McCoy ST, Rubin ES. An engineering-economic model of pipeline transport of CO2 with application to carbon capture and storage. International journal of greenhouse gas control 2008; 2(2): 219-29. https://doi.org/10.1016/S1750-5836(07)00119-3

[12] Witkowski A, Majkut M, Rulik S. Analysis of pipeline transportation systems for carbon dioxide sequestration. Archives of thermodynamics 2014; 35(1): 117-40. https://doi.org/10.2478/aoter-2014-0008

[13] De Visser E, Hendriks C, Barrio M, Mølnvik MJ, de Koeijer G, Liljemark S, Le Gallo Y. Dynamis CO2 quality recommendations. International journal of greenhouse gas control 2008; 2(4): 478-84. https://doi.org/10.1016/j.ijggc.2008.04.006

[14] Long A, Di X, Sun R, Sun X. Influencing factors of supercritical CO 2 transportation pipeline parameters. Oil & Gas Storage and Transportation 2013; 32(1): 15-9.

[15] Wang H, Chen J, Li Q. A review of pipeline transportation technology of carbon dioxide. InIOP conference series: earth and environmental science 2019; 310(3): 032033). IOP Publishing. https://doi.org/10.1088/1755-1315/310/3/032033

[16] Edwards RW, Celia MA. Infrastructure to enable deployment of carbon capture, utilization, and storage in the United States. Proceedings of the National Academy of Sciences 2018; 115(38): E8815-24. https://doi.org/10.1073/pnas.1806504115

[17] Oei PY, Herold J, Mendelevitch R. Modeling a carbon capture, transport, and storage infrastructure for Europe. Environmental Modeling & Assessment 2014; 19: 515-31. https://doi.org/10.1007/s10666-014-9409-3

[18] Young RJ, Lovell PA. Introduction to polymers. CRC press; 2011. https://doi.org/10.1201/9781439894156

[19] Ansaloni L, Alcock B, Peters TA. Effects of CO2 on polymeric materials in the CO2 transport chain: A review. International journal of greenhouse gas control 2020; 94: 102930. https://doi.org/10.1016/j.ijggc.2019.102930

[20] Takajo T, Takahara A, Kichikawa T. Surface modification of engineering plastics through swelling in supercritical carbon dioxide. Polymer journal 2008; 40(8): 716-24. https://doi.org/10.1295/polymj.PJ2007212

[21] Jiménez A, Thompson GL, Matthews MA, Davis TA, Crocker K, Lyons JS, Trapotsis A. Compatibility of medical-grade polymers with dense CO2. The Journal of supercritical fluids 2007; 42(3): 366-72. https://doi.org/10.1016/j.supflu.2007.05.002

[22] Sawan SP, Shieh YT, Su JH. Evaluation of the interactions between supercritical carbon dioxide and polymeric materials. Los Alamos, New Mexico: Los Alamos National Laboratory; 1994.

[23] Sawan SP, Shieh YT, Su JH, Manivannan G, Spall WD. Evaluation of supercritical fluid interactions with polymeric materials. InSupercritical Fluid Cleaning 1998; pp. 121-161. William Andrew Publishing. https://doi.org/10.1016/B978-081551416-9.50008-2

[24] Doroudiani S, Park CB, Kortschot MT. Effect of the crystallinity and morphology on the microcellular foam structure of semicrystalline polymers. Polymer Engineering & Science 1996; 36(21): 2645-62. https://doi.org/10.1002/pen.10664

[25] Michaels AS, Bixler HJ. Solubility of gases in polyethylene. Journal of Polymer Science 1961; 50(154): 393-412. https://doi.org/10.1002/pol.1961.1205015411

[26] Shieh YT, Su JH, Manivannan G, Lee PH, Sawan SP, Dale Spall W. Interaction of supercritical carbon dioxide with polymers. II. Amorphous polymers. Journal of applied polymer science 1996; 59(4): 707-17. https://doi.org/10.1002/(SICI)1097-4628(19960124)59:4<707::AID-APP16>3.0.CO;2-M

[27] Bos A, Pünt IG, Wessling M, Strathmann H. CO2-induced plasticization phenomena in glassy polymers. Journal of membrane science 1999; 155(1): 67-78. https://doi.org/10.1016/S0376-7388(98)00299-3

[28] Shieh YT, Su JH, Manivannan G, Lee PH, Sawan SP, Dale Spall W. Interaction of supercritical carbon dioxide with polymers. I. Crystalline polymers. Journal of applied polymer science 1996; 59(4): 695-705. https://doi.org/10.1002/(SICI)1097-4628(19960124)59:4<695::AID-APP15>3.0.CO;2-P

[29] Olsen CH, Augestad M, Helland I, Moldestad BM, Eikeland MS. Diffusion of CO2 through polymer membranes. WIT Trans. Ecol. Environ. 2020; 245: 211-22. https://doi.org/10.2495/EID200201

[30] Briscoe BJ, Savvas T, Kelly CT. "Explosive decompression failure" of rubbers: a review of the origins of pneumatic stress induced rupture in elastomers. Rubber chemistry and technology 1994; 67(3): 384-416. https://doi.org/10.5254/1.3538683

[31] Davies OM, Arnold JC, Sulley S. The mechanical properties of elastomers in high-pressure CO2. Journal of materials science 1999; 34: 417-22. https://doi.org/10.1023/A:1004442614090

[32] Paul S, Shepherd R, Woollin P. Selection of materials for high pressure CO2 transport. InThe Third International Forum on the Transportation of CO2 by Pipeline, paper 2012; 19: 1-16.

[33] Dubois J, Grau E, Tassaing T, Dumon M. On the CO2 sorption and swelling of elastomers by supercritical CO2 as studied by in situ high pressure FTIR microscopy. The Journal of Supercritical Fluids 2018; 131: 150-6. https://doi.org/10.1016/j.supflu.2017.09.003

[34] Lainé E, Grandidier JC, Benoit G, Omnès B, Destaing F. Effects of sorption and desorption of CO2 on the thermomechanical experimental behavior of HNBR and FKM O-rings-Influence of nanofiller-reinforced rubber. Polymer Testing 2019; 75: 298-311. https://doi.org/10.1016/j.polymertesting.2019.02.010

[35] Abas AZ, Mohammed Nor A, Suhor MF, Mat SA. Non-metallic materials in supercritical CO2 systems. InOffshore Technology Conference Asia 2014; pp. OTC-24963. OTC. https://doi.org/10.2118/24963-MS

[36] Kim SW, Sohn JS, Kim HK, Ryu Y, Cha SW. Effects of gas adsorption on the mechanical properties of amorphous polymer. Polymers 2019; 11(5): 817. https://doi.org/10.3390/polym11050817

[37] Bierwagen G, Huang Y. Development of Protective Coatings for Co-Sequestration Processes and Pipelines. North Dakota State Univ., Fargo, ND (United States); 2011. https://doi.org/10.2172/1053783

[38] Zakaria M, Sauri AS, Abas AZ, Mat S, Suhor MF, M Nor A, Kamarudin R. Assessment of Coatings in High pCO2 Environment for Pipeline Internal Coating Application. InOffshore Technology Conference Asia 2014; pp. OTC-25062. OTC. https://doi.org/10.4043/25062-MS

[39] Md Sauri AS, Zakaria M. Assessment of Internal Tubular Coating System for High CO2 Application. InICPER 2020: Proceedings of the 7th International Conference on Production, Energy and Reliability 2022; pp. 919-925. Singapore: Springer Nature Singapore. https://doi.org/10.1007/978-981-19-1939-8_68

[40] Zhang X, Zevenbergen JF, Spruijt MP, Borys M. Corrosion of pipe steel in CO2 containing impurities and possible solutions. Energy Procedia 2013; 37: 3147-59. https://doi.org/10.1016/j.egypro.2013.06.201

[41] Carrera MC, Erdmann E, Destéfanis HA. Barrier properties and structural study of nanocomposite of HDPE/montmorillonite modified with polyvinylalcohol. Journal of Chemistry 2013; 2013(1): 679567. https://doi.org/10.1155/2013/679567

[42] Cussler EL, Hughes SE, Ward III WJ, Aris R. Barrier membranes. Journal of membrane science 1988; 38(2): 161-74. https://doi.org/10.1016/S0376-7388(00)80877-7

[43] Van Westing EP, Ferrari GM, De Wit JH. The determination of coating performance using electrochemical impedance spectroscopy. Electrochimica acta 1994; 39(7): 899-910. https://doi.org/10.1016/0013-4686(94)85104-2

[44] Liu M, Jia Z, Jia D, Zhou C. Recent advance in research on halloysite nanotubes-polymer nanocomposite. Progress in polymer science 2014; 39(8): 1498-525. https://doi.org/10.1016/j.progpolymsci.2014.04.004

[45] Introzzi L, Blomfeldt TO, Trabattoni S, Tavazzi S, Santo N, Schiraldi A, Piergiovanni L, Farris S. Ultrasound-assisted pullulan/montmorillonite bionanocomposite coating with high oxygen barrier properties. Langmuir 2012; 28(30): 11206-14. https://doi.org/10.1021/la301781n

[46] Dunkerley E, Schmidt D. Effects of composition, orientation and temperature on the O2 permeability of model polymer/clay nanocomposites. Macromolecules 2010; 43(24): 10536-44. https://doi.org/10.1021/ma1018846

[47] Nyflött Å, Moons E, Bonnerup C, Carlsson G, Järnström L, Lestelius M. The influence of clay orientation and crystallinity on oxygen permeation in dispersion barrier coatings. Applied Clay Science 2016; 126: 17-24. https://doi.org/10.1016/j.clay.2016.02.029

[48] Bhunia K, Dhawan S, Sablani SS. Modeling the Oxygen Diffusion of Nanocomposite-based Food Packaging Films. Journal of food science 2012; 77(7): N29-38. https://doi.org/10.1111/j.1750-3841.2012.02768.x

[49] Mittal V. Modelling and prediction of barrier properties of polymer layered silicate nanocomposites. Polymers and Polymer Composites 2013; 21(8): 509-18. https://doi.org/10.1177/096739111302100804

[50] Loryuenyong V, Saewong C, Aranchaiya C, Buasri A. The improvement in mechanical and barrier properties of poly (vinyl alcohol)/graphene oxide packaging films. Packaging Technology and Science 2015; 28(11): 939-47. https://doi.org/10.1002/pts.2149

[51] Noshirvani N, Ghanbarzadeh B, Fasihi H, Almasi H. Starch–PVA nanocomposite film incorporated with cellulose nanocrystals and MMT: a comparative study. International Journal of Food Engineering 2016; 12(1): 37-48. https://doi.org/10.1515/ijfe-2015-0145

[52] Cairns MJ, Mesic B, Johnston JH, Herzog MB. Use of spherical silica particles to improve the barrier performance of coated paper. Nordic Pulp & Paper Research Journal 2019; 34(3): 334-42. https://doi.org/10.1515/npprj-2018-0066

[53] Cairns MJ, Mesic B, Johnston JH, Hill SJ, Kirby N. Tetraethylorthosilicate-containing barrier dispersion coatings—Mechanism of action. Progress in Organic Coatings 2020; 139: 105443. https://doi.org/10.1016/j.porgcoat.2019.105443

[54] Chen B, Evans JR, Greenwell HC, Boulet P, Coveney PV, Bowden AA, Whiting A. A critical appraisal of polymer–clay nanocomposites. Chemical Society Reviews 2008; 37(3): 568-94. https://doi.org/10.1039/B702653F

[55] Ray SS, Okamoto M. Polymer/layered silicate nanocomposites: a review from preparation to processing. Progress in polymer science 2003; 28(11): 1539-641. https://doi.org/10.1016/j.progpolymsci.2003.08.002

[56] Bharadwaj RK. Modeling the barrier properties of polymer-layered silicate nanocomposites. Macromolecules 2001; 34(26): 9189-92. https://doi.org/10.1021/ma010780b

[57] Dai CF, Li PR, Yeh JM. Comparative studies for the effect of intercalating agent on the physical properties of epoxy resin-clay based nanocomposite materials. European Polymer Journal 2008; 44(8): 2439-47. https://doi.org/10.1016/j.eurpolymj.2008.06.015

[58] Yeh JM, Chin CP, Chang S. Enhanced corrosion protection coatings prepared from soluble electronically conductive polypyrrole-clay nanocomposite materials. Journal of Applied Polymer Science 2003; 88(14): 3264-72. https://doi.org/10.1002/app.12146

[59] Olad A, Rashidzadeh A, Amini M. Preparation of polypyrrole nanocomposites with organophilic and hydrophilic montmorillonite and investigation of their corrosion protection on iron. Advances in polymer technology 2013; 32(2). https://doi.org/10.1002/adv.21337

[60] Tomić MD, Dunjić B, Likić V, Bajat J, Rogan J, Djonlagić J. The use of nanoclay in preparation of epoxy anticorrosive coatings. Progress in organic coatings 2014; 77(2): 518-27. https://doi.org/10.1016/j.porgcoat.2013.11.017

[61] Piromruen P, Kongparakul S, Prasassarakich P. Synthesis of polyaniline/montmorillonite nanocomposites with an enhanced anticorrosive performance. Progress in Organic Coatings 2014; 77(3): 691-700. https://doi.org/10.1016/j.porgcoat.2013.12.007

[62] Chang KC, Chen ST, Lin HF, Lin CY, Huang HH, Yeh JM, Yu YH. Effect of clay on the corrosion protection efficiency of PMMA/Na+-MMT clay nanocomposite coatings evaluated by electrochemical measurements. European Polymer Journal 2008; 44(1): 13-23. https://doi.org/10.1016/j.eurpolymj.2007.10.011

[63] Raju A, Lakshmi V, Prataap RV, Resmi VG, Rajan TP, Pavithran C, Prasad VS, Mohan S. Adduct modified nano-clay mineral dispersed polystyrene nanocomposites as advanced corrosion resistance coatings for aluminum alloys. Applied Clay Science 2016; 126: 81-8. https://doi.org/10.1016/j.clay.2016.03.005

[64] Huang HY, Huang TC, Yeh TC, Tsai CY, Lai CL, Tsai MH, Yeh JM, Chou YC. Advanced anticorrosive materials prepared from amine-capped aniline trimer-based electroactive polyimide-clay nanocomposite materials with synergistic effects of redox catalytic capability and gas barrier properties. Polymer 2011; 52(11): 2391-400. https://doi.org/10.1016/j.polymer.2011.03.030

[65] Sugama T. Polyphenylenesulfied/montomorillonite clay nanocomposite coatings: Their efficacy in protecting steel against corrosion. Materials Letters 2006; 60(21-22): 2700-6. https://doi.org/10.1016/j.matlet.2006.01.111

[66] Hu J, Gan M, Ma L, Li Z, Yan J, Zhang J. Synthesis and anticorrosive properties of polymer–clay nanocomposites via chemical grafting of polyaniline onto Zn-Al layered double hydroxides. Surface and Coatings Technology 2014; 240: 55-62. https://doi.org/10.1016/j.surfcoat.2013.12.012

[67] Manninen AR, Naguib HE, Nawaby AV, Day M. CO2 sorption and diffusion in polymethyl methacrylate–clay nanocomposites. Polymer Engineering & Science 2005; 45(7): 904-14. https://doi.org/10.1002/pen.20350

[68] Guo Z, Lee LJ, Tomasko DL. CO2 permeability of polystyrene nanocomposites and nanocomposite foams. Industrial & engineering chemistry research 2008; 47(23): 9636-43. https://doi.org/10.1021/ie8000088

[69] Hu D, Chen J, Sun S, Liu T, Zhao L. Solubility and diffusivity of CO2 in isotactic polypropylene/nanomontmorillonite composites in melt and solid states. Industrial & Engineering Chemistry Research 2014; 53(7): 2673-83. https://doi.org/10.1021/ie403580x

[70] Yoo BM, Shin HJ, Yoon HW, Park HB. Graphene and graphene oxide and their uses in barrier polymers. Journal of Applied Polymer Science 2014; 131(1). https://doi.org/10.1002/app.39628

[71] Ouyang X, Huang W, Cabrera E, Castro J, Lee LJ. Graphene-graphene oxide-graphene hybrid nanopapers with superior mechanical, gas barrier and electrical properties. Aip Advances 2015; 5(1). https://doi.org/10.1063/1.4906795

[72] Roilo D. Gas transport properties and free volume structure of polymer nanocomposite membranes. Doctoral Thesis, University of Trento, Department of Physics, 2017.

[73] Klopffer MH, Flaconneche B. Transport properties of gases in polymers: bibliographic review. Oil & Gas Science and Technology 2001; 56(3): 223-44. https://doi.org/10.2516/ogst:2001021

[74] Benjelloun-Dabaghi Z, Benali A. Mathematical modelling of the permeation of gases in polymers. Oil & Gas Science and Technology 2001; 56(3): 295-303. https://doi.org/10.2516/ogst:2001025

[75] Flaconnèche B, Martin J, Klopffer MH. Permeability, diffusion and solubility of gases in polyethylene, polyamide 11 and poly (vinylidene fluoride). Oil & Gas Science and Technology 2001; 56(3): 261-78. https://doi.org/10.2516/ogst:2001023

[76] Flaconnèche B, Martin J, Klopffer MH. Transport properties of gases in polymers: experimental methods. Oil & gas science and technology 2001; 56(3): 245-59. https://doi.org/10.2516/ogst:2001022

[77] Rogers CE. Permeation of gases and vapours in polymers. InPolymer permeability 1985; pp. 11-73. Dordrecht: Springer Netherlands. https://doi.org/10.1007/978-94-009-4858-7_2

[78] Klopffer MH, Flaconneche B, Odru P. Transport properties of gas mixtures through polyethylene. Plastics, Rubber and Composites 2007; 36(5): 184-9. https://doi.org/10.1179/174328907X191350

[79] Tobolsky AV, Mark HF. Polymer science and materials. AV Tobolsky and HF Mark eds, Wiley-Interscience, New York, NY 1971.

[80] Crank J. The mathematics of diffusion. Oxford university press; 1979.

[81] Karimi M. Diffusion in polymer solids and solutions. Mass transfer in chemical engineering processes 2011; 25: 17. https://doi.org/10.5772/23436

[82] Neogi P. Transport Phenomena in Polymer. Diffusion in polymers 1996; 32: 173.

[83] Naylor TD. Permeation properties, Comprehensive Polymer Science, 1989; 2Pergamon Press. https://doi.org/10.1016/B978-0-08-096701-1.00057-4

[84] Rogers CE. Permeability and chemical resistance. Engineering design for plastics 1964: 609-88.

[85] Mulder M. Basic principles of membrane technology. Springer science & business media; 2012.

[86] McKeen LW. Film properties of plastics and elastomers. William Andrew; 2017.

[87] Cui Y, Kumar S, Kona BR, van Houcke D. Gas barrier properties of polymer/clay nanocomposites. Rsc Advances 2015; 5(78): 63669-90. https://doi.org/10.1039/C5RA10333A

[88] Picard E, Vermogen A, Gérard JF, Espuche E. Barrier properties of nylon 6-montmorillonite nanocomposite membranes prepared by melt blending: Influence of the clay content and dispersion state: Consequences on modelling. Journal of Membrane Science 2007; 292(1-2): 133-44. https://doi.org/10.1016/j.memsci.2007.01.030

[89] Maxwell JC. A treatise on electricity and magnetism. Clarendon press; 1873.

[90] Tu Z, Mao J, Mao J, Jiang H. A novel determination of the minimal size of a probabilistic representative volume element for fiber-reinforced composites' thermal analysis. Thermal Science 2018; 22(6 Part A): 2551-64. https://doi.org/10.2298/TSCI160430222T

[91] Nielsen LE. Models for the permeability of filled polymer systems. Journal of Macromolecular Science—Chemistry 1967; 1(5): 929-42. https://doi.org/10.1080/10601326708053745

[92] Cussler EL, Hughes SE, Ward III WJ, Aris R. Barrier membranes. Journal of membrane science 1988; 38(2): 161-74. https://doi.org/10.1016/S0376-7388(00)80877-7

[93] Duncan TV. Applications of nanotechnology in food packaging and food safety: barrier materials, antimicrobials and sensors. Journal of colloid and interface science 2011; 363(1): 1-24. https://doi.org/10.1016/j.jcis.2011.07.017

[94] Nazari MH, Zhang Y, Mahmoodi A, Xu G, Yu J, Wu J, Shi X. Nanocomposite organic coatings for corrosion protection of metals: A review of recent advances. Progress in Organic Coatings 2022; 162: 106573. https://doi.org/10.1016/j.porgcoat.2021.106573

[95] Nguyen-Tri P, Nguyen TA, Carriere P, Ngo Xuan C. Nanocomposite coatings: preparation, characterization, properties, and applications. International Journal of Corrosion 2018; 2018(1): 4749501. https://doi.org/10.1155/2018/4749501

[96] Sanchez C, Belleville P, Popall M, Nicole L. Applications of advanced hybrid organic–inorganic nanomaterials: from laboratory to market. Chemical Society Reviews 2011; 40(2): 696-753. https://doi.org/10.1039/c0cs00136h

[97] Facio DS, Mosquera MJ. Simple strategy for producing superhydrophobic nanocomposite coatings in situ on a building substrate. ACS Applied Materials & Interfaces 2013; 5(15): 7517-26. https://doi.org/10.1021/am401826g

[98] Toledano R, Mandler D. Electrochemical codeposition of thin gold nanoparticles/sol− gel nanocomposite films. Chemistry of Materials 2010; 22(13): 3943-51. https://doi.org/10.1021/cm1005295

[99] Golgoon A, Aliofkhazrae M, Toorani M. Nanocomposite protective coatings fabricated by electrostatic spray method. Protection of Metals and Physical Chemistry of Surfaces 2018; 54: 192-221. https://doi.org/10.1134/S207020511802017X

[100] Yang Q, Ma Y, Zhu J, Chow K, Shi K. An update on electrostatic powder coating for pharmaceuticals. Particuology 2017; 31: 1-7. https://doi.org/10.1016/j.partic.2016.10.001

[101] Pierson HO. Handbook of chemical vapor deposition: principles, technology and applications. William Andrew; 1999. https://doi.org/10.1016/B978-081551432-9.50005-X

[102] Bogdanovic U, Vodnik V, Mitric M, Dimitrijevic S, Skapin SD, Zunic V, Budimir M, Stoiljkovic M. Nanomaterial with high antimicrobial efficacy copper/polyaniline nanocomposite. ACS applied materials & interfaces 2015; 7(3): 1955-66. https://doi.org/10.1021/am507746m

[103] Zhang S, Sun G, He Y, Fu R, Gu Y, Chen S. Preparation, characterization, and electrochromic properties of nanocellulose-based polyaniline nanocomposite films. ACS Applied Materials & Interfaces 2017; 9(19): 16426-34. https://doi.org/10.1021/acsami.7b02794

[104] Shabani-Nooshabadi M, Ghoreishi SM, Jafari Y, Kashanizadeh N. Electrodeposition of polyaniline-montmorrilonite nanocomposite coatings on 316L stainless steel for corrosion prevention. Journal of Polymer Research 2014; 21: 1-0. https://doi.org/10.1007/s10965-014-0416-5

[105] Chen F, Wan P, Xu H, Sun X. Flexible transparent supercapacitors based on hierarchical nanocomposite films. ACS applied materials & interfaces 2017; 9(21): 17865-71. https://doi.org/10.1021/acsami.7b02460

[106] Kaboorani A, Auclair N, Riedl B, Landry V. Mechanical properties of UV-cured cellulose nanocrystal (CNC) nanocomposite coating for wood furniture. Progress in Organic Coatings 2017; 104: 91-6. https://doi.org/10.1016/j.porgcoat.2016.11.031

[107] Villafiorita-Monteleone F, Canale C, Caputo G, Cozzoli PD, Cingolani R, Fragouli D, Athanassiou A. Controlled swapping of nanocomposite surface wettability by multilayer photopolymerization. Langmuir 2011; 27(13): 8522-9. https://doi.org/10.1021/la2017402

[108] Hsu SH, Chang YL, Tu YC, Tsai CM, Su WF. Omniphobic low moisture permeation transparent polyacrylate/silica nanocomposite. ACS Applied Materials & Interfaces 2013; 5(8): 2991-8. https://doi.org/10.1021/am302446t

[109] Talib RJ, Saad S, Toff MR, Hashim H. Thermal spray coating technology: A review. Solid State Sci Technol 2003; 11(1): 109-17.

[110] Boddula R, Ahamed MI, Asiri AM, editors. Polymers Coatings: Technology and Applications. John Wiley & Sons; 2020.

[111] Atay HY. Fabrication methods for polymer coatings. Polymer Coatings: Technology and Applications 2020; 1-20. https://doi.org/10.1002/9781119655145.ch1

Received on 10-05-2025 Accepted on 06-06-2025 Published on 04-07-2025

https://doi.org/10.6000/1929-5995.2025.14.08